Catal Lett (2008) 126:31–35
DOI 10.1007/s10562-008-9643-x

When an Encapsulating Oxide Layer Promotes Reaction on Noble Metals: Dewetting and In situ Formation of an "Inverted" FeO_x/Pt Catalyst

Ying-Na Sun · Zhi-Hui Qin · Mikolaj Lewandowski · Sarp Kaya · Shamil Shaikhutdinov · Hans-Joachim Freund

Received: 24 June 2008 / Accepted: 2 September 2008 / Published online: 7 October 2008

Abstract An ultra-thin FeO(111) film grown on Pt(111) is found to exhibit a much higher rate of CO oxidation at stoichiometric CO:O_2 ratios than the clean Pt(111) surface. This unexpected result is rationalized on the basis of reaction induced dewetting of the oxide film, ultimately resulting in highly dispersed FeO_x nanoparticles on Pt(111). The effect may have a strong impact on the catalytic properties of the noble metal particles encapsulated by the reducible oxide support as a result of strong metal-support interaction.

Keywords Platinum · Iron oxides · Strong metal-support interaction · CO oxidation · Surface restructuring · Selective oxidation

1 Introduction

Metals supported on reducible oxides often exhibit strong metal-support interaction (SMSI) [1, 2] which in many cases manifests itself by encapsulation (decoration) of the metal particles by a thin oxide film. Formation of a TiO_x ($x \sim 1$) layer on Pt and Pd particles supported on TiO_2 upon heating to high temperatures (>773 K) in a reducing atmosphere is a well-known example in the literature [3–7]. Although generalizations are not straightforward for the SMSI effects, it is rather obvious that decoration will suppress catalytic activity and be particularly detrimental for the metal surface structure sensitive reactions in contrast to the structure insensitive ones [2, 8–10]. Certainly, this conclusion implies that the encapsulated layer is inert in the reaction and remains unchanged. On the other hand, the partial reversal of the SMSI state has been suggested to occur during the CO hydrogenation reaction on Pt/TiO_2 [11, 12], thus indicating that the SMSI effects are not responsible for the enhanced activity as originally proposed [13]. This finding in turn raises the question, how could one envision such a reversal and how could this lead to a higher activity in the absence of SMSI?

In this letter, we demonstrate that a thin film of transition metal oxide fully covering a noble metal surface upon preparation exhibits a strong promoting effect on the oxidation reaction. More specifically, we have found that a FeO(111) film grown on Pt(111) shows a much higher reaction rate in CO oxidation under oxygen lean conditions than clean Pt(111). This unexpected result is rationalized in terms of reaction induced dewetting of the oxide film, ultimately resulting in the formation of iron oxide nanoparticles dispersed on the Pt(111) surface, whereby the reaction takes place at the oxide/metal interface. Since the same FeO layer is formed on the Pt particles supported on iron oxide as a result of SMSI upon high temperature annealing [14], we are effectively forming a structure, referred to as "inverted model catalyst" [15] to differentiate it from systems where metal particles are supported on oxide surface.

CO oxidation on Pt is one of the most studied reactions in catalysis on metals (see reviews [16–18]) that proceed via the Langmuir–Hinshelwood mechanism whereby CO_2 is formed through the associative reaction of chemisorbed CO with the oxygen surface atoms produced by dissociation of molecular oxygen. The reaction has two distinct branches in the kinetic phase diagram, which are determined by the CO:O_2 ratio, reflecting the competition for

Y.-N. Sun · Z.-H. Qin · M. Lewandowski · S. Kaya · S. Shaikhutdinov (✉) · H.-J. Freund
Department of Chemical Physics, Fritz-Haber-Institute der Max-Plank-Gesellschaft, Faradayweg 4-6, 14195 Berlin, Germany
e-mail: shamil@fhi-berlin.mpg.de

adsorption sites between O_2 and CO. Under oxygen rich conditions ($CO:O_2 < 0.2$), the metal surface is covered by oxygen, which does not affect adsorption of the CO that readily reacts with oxygen. In contrast, the reaction exhibits low activity in excess of CO which suppresses oxygen dissociation due to site blocking. In addition, spatio-temporal oscillations were found on Pt, in particular on the more open Pt(100) and Pt(110) surfaces exhibiting surface reconstructions [19–24]. On the Pt(111) surface no such oscillations were observed at the low pressures commonly used in surface science experiments. Meanwhile the CO + O surface phase diagram shows a bistability region between high and low reactivity states, which is accompanied by a hysteresis in the reaction rate [24–27]. However, the oscillatory kinetics of the CO oxidation rate on Pt(111) were found at elevated pressures (10^{-3}–1 mbar O_2) and interpreted in terms of oxidation reduction cycles of the Pt surface [27].

For reactivity studies at low pressures we employed temperature programmed desorption and reaction (TPD, TPR) techniques in an ultra-high vacuum (UHV) chamber. The experiments, at elevated pressures of up to 1 bar with gas chromatography (GC) analysis of products, were carried out on the same sample in the so-called "high-pressure cell" used as a circulating flow reactor, which is sealed from the main UHV chamber by a Viton O-ring (see Sect. 2). The preparation and the atomic structure of the ultra-thin FeO(111) film on Pt(111) is well documented in the literature [28]. The film consists of close-packed layers of iron and oxygen stacked as O–Fe–Pt(111).

Figure 1 shows the CO_2 production measured over the Pt(111) and FeO/Pt(111) samples at 450 K in 40 mbar CO + 20 mbar O_2 balanced by He to 1 bar. It is not surprising that in excess of CO the Pt(111) surface exhibits low activity due to the site blocking effect mentioned above. What is unexpected is that the FeO covered surface oxidizes CO with a much higher rate than clean Pt. Quite the contrary, one would have expected that the FeO film further suppresses the reaction on Pt. Indeed, the TPD and TPR studies revealed no CO_2 formation on the FeO(111) film since neither CO nor O_2 chemisorbs on this surface. In addition, no structural changes were observed after long-time exposure to 10^{-6} mbar CO or O_2 at 450 K.

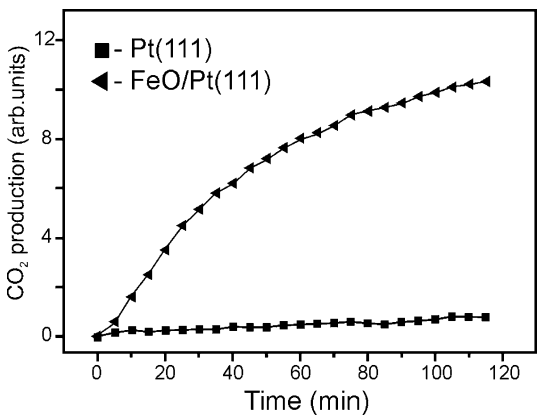

Fig. 1 Production of CO_2 over Pt(111) and FeO(111)/Pt(111) samples at 450 K in the mixture of 40 mbar CO and 20 mbar O_2 balanced by He. Time zero corresponds to the start of the sample heating, which takes ~3 min to reach the reaction temperature

In order to shed light on the structure of the FeO/Pt model catalysts during the reaction at elevated pressures, we have performed post-characterization of the samples in UHV using low energy electron diffraction (LEED), Auger electron spectroscopy (AES) and TPD. For this, the crystal is rapidly cooled down to room temperature, and the reactor is pumped out down to $\sim 10^{-5}$ mbar before exposing it to the UHV chamber.

Figure 2a shows LEED patterns of the FeO/Pt(111) surface as prepared and after 120 min in the reaction. The flower-like diffraction spots obtained on the original FeO film is characteristic for the Moire superstructure due to the

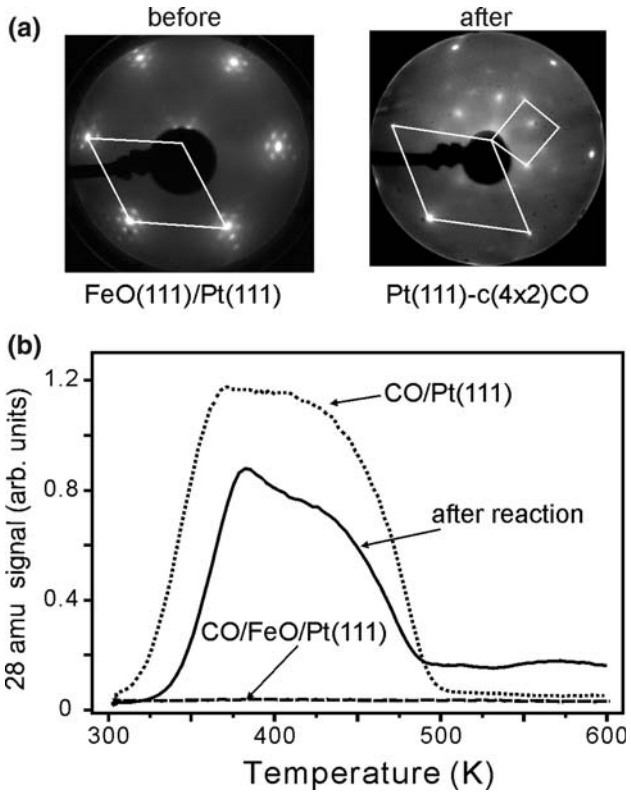

Fig. 2 (**a**) LEED patterns ($E = 60$ eV) of the FeO(111)/Pt(111) surface before and after CO oxidation reaction for 120 min. After the reaction the pattern is assigned to the Pt(111)–c(4 × 2)CO structure. The unit cells of FeO(111) (left) and Pt(111) (right) are indicated. The rectangular c(4 × 2) unit cell is shown only for one domain. (**b**) TPD spectra of CO adsorbed at 300 K on the clean Pt(111) (dotted line) and FeO(111)/Pt(111) (dashed line) surfaces. The solid line represents the spectrum of CO desorbing upon heating of the FeO/Pt sample taken after 120 min on stream

~10% lattice mismatch between FeO(111) and Pt(111) [28]. Meanwhile, the surface of the used sample does not show the Moire structure, but rather the sharp Pt(111)-(1 × 1) spots with additional weak spots, which can be assigned to a Pt(111)–c(4 × 2)CO structure, well established for the adsorption of CO on clean Pt(111) [29–31] and confirmed in our own experiments. The observation of the ordered structure by LEED points out that the surface of the used samples exposes a significant fraction of Pt(111).

Only CO and CO_2 were found as desorbing species upon heating of the used samples to 800 K. The amount of CO adsorbed on these samples turned out to be 30–40% lower than that measured by CO adsorption on the clean Pt(111), and the desorption profile looks very similar to CO on Pt(111) (see Fig. 2b), which is consistent with the above LEED results. Interestingly, subsequent UHV annealing at $T > 800$ K essentially restores the LEED pattern of the original FeO film and makes the samples again inert towards CO. This means that the iron oxide is not consumed during the reaction through the formation of any volatile compounds.

The AES study of the used catalysts revealed only small amounts of carbon beyond the elements, which belong to the original surfaces. In particular, no nickel (via Ni carbonyls) has been detected which may contaminate CO gas in stainless steel high-pressure containers. The carbon observed in the AES spectra on both the Pt(111) and FeO/Pt(111) samples most probably originates from the CO dissociation on the Pt low coordination sites such as step edges. Using the O:Fe signal ratio in the original FeO films as a reference, we found that the iron oxide phase in the used samples exhibits a $FeO_{1.3}$ stoichiometry, i.e., close to Fe_3O_4. Again, annealing to 800 K in UHV restores the O:Fe ratio in the Auger spectra, i.e., consistent with the above LEED data.

Surface morphology of the model catalysts was studied by scanning tunneling microscopy (STM). The experiments were carried out in another UHV chamber connected via gate valve to a gold-plated high-pressure cell, here used as a batch reactor at the same reaction conditions as in the previous experiments. Figure 3 shows that the original FeO(111) film with atomically flat, wide terraces transforms into the system represented by small particles randomly distributed on the substrate (cf. Fig. 3a, b). The particles show a narrow size distribution of 8 ± 1 nm in diameter and 1.8 ± 0.1 nm in height. Based on the above LEED and AES results, these nanoparticles can straightforwardly be assigned to the iron oxide particles. Meanwhile, the Pt(111) surface essentially maintains the crystal morphology after 120 min in the reaction (see Fig. 3c). Only small, irregularly shaped particles, presumably of carbon (as judged by AES), and primarily at the steps are observed by STM.

Thus, combined LEED, AES, TPD and STM studies clearly show that the working catalyst does not expose the FeO(111) film but Pt(111) covered by FeO_x nanoparticles. Additional experiments with pure oxygen and CO at the same partial pressures did not reveal such a transformation. Therefore, the results suggest that a massive surface reconstruction occurs during the CO oxidation reaction at elevated pressures. Apparently, the reaction induces dewetting of the original thin FeO film into the more oxygen rich iron oxide particles, which may again wet the Pt surface by heating in a reducing (vacuum) atmosphere.

These wetting/dewetting phenomena observed are thermodynamically driven. The formation of the FeO(111) thin film wetting the Pt(111) substrate in vacuum is a result of decreasing surface energy since oxides usually exhibit the lower surface energy than metals [32]. However, the situation changes under reaction conditions, since it includes also chemical potentials of the gas phase, which in turn depends on partial pressure and temperature. In addition, kinetics of the transformations, which are intimately linked to the (oxidation) reaction, may also influence the wetting/dewetting processes observed. In principle, the most stable surface structure can be predicted on the basis of the so-called stability plot calculated by density functional theory (e.g., see Ref. [33]). However, this information is not available for the present system.

Although the experimental results presented here do not allow us to determine the details of the reaction mechanism, it is clear that the reaction does not occur on the Pt surface, which becomes accessible upon dewetting of the FeO film. At the stoichiometric $CO:O_2$ ratio used, the

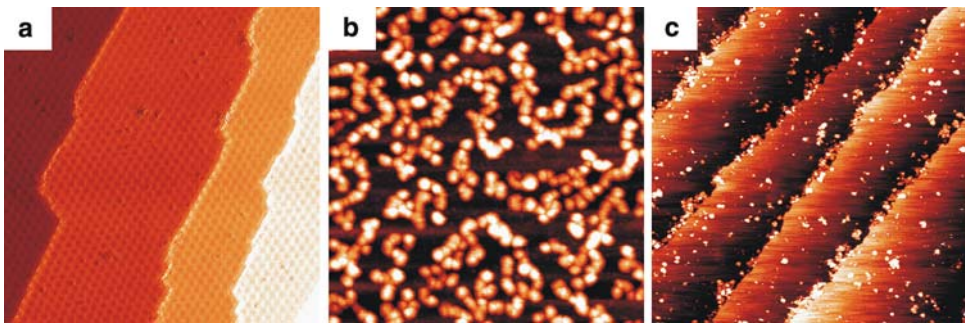

Fig. 3 Room temperature STM images (size 200 × 200 nm^2) of clean FeO(111)/Pt(111) surface (**a**), FeO(111)/Pt(111) (**b**), and Pt(111) (**c**) surfaces after 120 min in the CO oxidation reaction at 450 K. Tunneling parameters are: bias 0.2 V, current 1 nA (**a**); 0.8 V, 0.5 nA (**b**); 0.5 V, 0.3 nA (**c**)

reaction on Pt(111) is self-poisoned by CO and therefore exhibits low activity (see Fig. 1). In principle, the iron oxide particles covering the Pt substrate in fact reduce the average size of the Pt domains between the particles, which in turn might shift the transition between the high and the low reaction rate branches to the higher $CO:O_2$ ratio as recently found for alumina supported Pd particles [34]. However, this effect can hardly be responsible for the enhanced reactivity in our case since this transition and reaction bistability on Pt(111), even in the mbar pressure range, occurs at much lower $CO:O_2$ ratios and temperatures (e.g., $\sim$0.01 at 410 K [27]) than used in our study.

On the other hand, we did not observe any substantial activity on the nm-thick, well-ordered $Fe_3O_4(111)$ films grown on Pt(111). In addition, the used samples, which were pre-flashed to 500 K to desorb any species re-adsorbed while cooling and pumping out the reactor, showed CO TPD spectra very similar to CO on Pt(111), albeit of lower intensity (not shown here). In other words, iron oxide particles formed during the reaction (see Fig. 3) practically do not adsorb CO at the reaction temperature (450 K). Therefore, the results indicate that the reaction does not occur on the iron oxide particles either. Thus we conclude that the CO oxidation reaction takes place at the perimeter of the iron oxide particles, which provide oxygen to CO adsorbing on the Pt surface.

The results presented above may aid in our understanding of the catalytic properties of metal particles supported on reducible oxide like iron oxide. For example, iron oxides have recently been shown to exhibit a strong promoting effect on the Pt/Al_2O_3 catalysts in the selective oxidation of CO in H_2 (PROX technology) used in the proton exchange membrane fuel cells [35–37]. Farrauto and co-workers suggested that the iron oxide being in intimate contact with the Pt particles provides oxygen for the CO adsorbed on the Pt surface [36]. Later, Tanaka and co-workers [37] found that the activity and selectivity of Pt catalysts in the PROX reaction can be significantly improved by depositing iron oxide in amounts $\sim$100 times exceeding that of Pt, i.e., implying that Pt is totally covered by FeO_x phase. The role of iron oxide in this case is still puzzling [37]. However, our results suggest that under reaction conditions the iron oxide covering Pt surface may dewet and thus open the Pt surface. If so, the reaction could undergo the dual mechanism suggested by Farrauto and co-workers [34].

In summary, we have found that the Pt(111) crystal fully covered by a thin FeO film exhibits enhanced activity in CO oxidation under oxygen lean conditions. The effect is explained by the dewetting of the film that occurs only at elevated pressures (in the 10 mbar range). Therefore, the catalytic reaction in fact proceeds over the so-called "inverted catalyst" where iron oxide nanoparticles are supported on Pt, i.e., in contrast to the oxide supported Pt particles. The reaction most likely occurs at the oxide/metal interface where iron oxide provides oxygen for CO adsorbing on Pt. We believe that the reaction induced dewetting observed here may have a strong impact on the catalytic properties of the metal particles encapsulated by a thin oxide layer as a result of SMSI.

1.1 Experimental Section

The experiments were performed in two UHV chambers (TPD–GC and STM) equipped with LEED, AES and a quadrupole mass spectrometer (QMS). The TPD–GC chamber houses a high-pressure reactor ($\sim$30 mL, made of Cu block) connected to gas handling lines and a gas chromatograph 6890N (from Agilent). The Pt(111) crystal ($\sim$10 mm in diameter, 1.5 mm in thickness, from Mateck) is spot-welded to two parallel Ta wires which are in turn welded to two Ta sticks used for resistive heating and also for cooling by filling a manipulator rod with liquid nitrogen. The temperature is measured by a chromel–alumel thermocouple spot-welded to the backside of the crystal and controlled using a feedback control system (Schlichting Phys. Instrum.). The manipulator rod inside the chamber ends with a KF-type flange with a four pin electrical feed through holding Ta and thermocouple sticks. The reactor is well-sealed with a Viton O-ring placed on top of the reactor matching the flange on the rod.

In the STM chamber, the Pt(111) crystal is mounted to a Pt sample holder. The temperature is controlled using a chromel–alumel thermocouple spot-welded to the edge of the crystal. The crystal can be heated in the UHV chamber by electron bombardment from the backside using a tungsten filament. For treatments at high pressures the sample is transferred into the gold-plated reactor ($\sim$1 l) housing a heating stage, consisting of only ceramic and sapphire pieces. The sample is heated radiatively from the backside using a halogen lamp.

The FeO(111) films are grown by physical vapor deposition of one monolayer of Fe (99.95%, Goodfellow) onto clean Pt(111) at 300 K and subsequent annealing in 10^{-6} mbar O_2 at 1,000 K for 2 min [28].

For high-pressure experiments, CO (99.995%, Linde) and O_2 (99.999%, AGA GmbH) were additionally cleaned using a cold trap at $\sim$200 K. The reaction mixture consists of 40 mbar CO and 20 mbar O_2 balanced by He to 1 bar. The gas was circulating through the reactor with a flow of 3 mL/min and analyzed by GC (HP-Plot Q column at 35°, TCD detector). The CO conversion in these experiments was below 1% even after 120 min on stream, excluding the effect of feedstock composition changes on global reactivity.

Acknowledgments We acknowledge support from DFG through SFB546 ("Transition metal oxides") and the Cluster of Excellence

UNICAT, coordinated by TU Berlin, and the Fonds der Chemischen Industrie.

References

1. Tauster SJ, Fung SC, Garten RL (1978) J Am Chem Soc 100:170
2. Tauster SJ (1987) Acc Chem Res 20:389
3. Pesty F, Steinrück HP, Madey TE (1995) Surf Sci 339:83
4. Dulub O, Hebenstreit W, Diebold U (2000) Phys Rev Lett 84:3646
5. Jennison DR, Dulub O, Hebenstreit W, Diebold U (2001) Surf Sci 492:L677
6. Bowker M, Stone P, Morrall P, Smith R, Bennett R, Perkins N, Kvon R, Pang C, Fourre E, Hall M (2005) J Catal 234:172
7. Silly F, Castell MR (2005) J Phys Chem B 109:12316
8. Haller GL, Resasco DE (1989) Adv Catal 36:173
9. Ko E, Garten R (1981) J Catal 68:223
10. Haller GL (2003) J Catal 216:12
11. Blankenburg KJ, Datye AK (1991) J Catal 128:186
12. Datye AK, Kalakkad DS, Yao MH, Smith DJ (1995) J Catal 155:148
13. Vannice MA, Twu CC (1983) J Catal 82:213
14. Qin ZH, Lewandowski M, Sun YN, Shaikhutdinov S, Freund HJ J Phys Chem C (in press)
15. Hayek K, Fuchs M, Klötzer B, Reichl W, Rupprechter G (2000) Topics Catal 13:55
16. Engel T, Ertl G (1979) Adv Catal 28:1
17. Berlowitz PJ, Peden CHF, Goodman DW (1988) J Phys Chem 90:5213
18. Santra AK, Goodman DW (2002) Electrochimica Acta 47:3595
19. Eiswirth M, Ertl G (1986) Surf Sci 177:90
20. Norton PR, Bindner PE, Griffiths K, Jackman TE, Davies JA, Rustig J (1984) J Chem Phys 80:3859
21. Vishnevskii A, Savchenko V (1989) React Kinet Catal Lett 38:167
22. Yeates RC, Turner JE, Gellman AJ, Somorjai GA (1985) Surf Sci 149:175
23. Imbihl R, Ertl G (1995) Chem Rev 95:697
24. Zhdanov VP, Kasemo B (1994) Surf Sci Rep 20:113
25. Berdau M, Yelenin GG, Karpowicz A, Ensasi M, Christmann K, Block JH (1999) J Chem Phys 110:11552
26. Colen RER, Christoph J, Pena F, Rotermund HH (1998) Surf Sci 408:310
27. Ritter M, Ranke W, Weiss W (1998) Phys Rev B 57:7240
28. Morgan AE, Somorjai GA (1969) J Chem Phys 51:3309
29. Ogletree DF, van Hove MA, Somorjai GA (1986) Surf Sci 173:351
30. Steininger H, Lehwald S, Ibach H (1982) Surf Sci 123:264
31. Johanek V, Laurin M, Grant AW, Kasemo B, Henry CR, Libuda J (2004) Science 304:1639
32. Kolodziejczyk M, Colen RER, Berdau M, Delmon B, Block JH (1997) Surf Sci 375:235
33. Korotkikh O, Farrauto R (2000) Catal Today 62:249
34. Liu X, Korotkikh O, Farrauto R (2002) Appl Catal A: Gen 226:293
35. Tanaka K-I, Morooka Y, Ishigure K, Yajima T, Okabe Y, Kato Y, Hamano H, Sekiya S-I, Tanaka H, Matsumoto Y, Koinuma H, He H, Zhang C, Feng Q (2004) Catal Lett 92:115
36. Sirijaruphan A, Goodwin JG Jr, Rice RW (2004) J Catal 224:304
37. Shi X, Tanaka K-I, He H, Shou M, Xu W, Zhang X (2008) Catal Lett 120:210